Weakly compressible Lattice Boltzmann simulations of reacting flows with detailed thermo-chemical models

Sa Hosseini,, Amir Eshghinejad-Fard,, Nasser Darabiha, D. Thevenin,

Version of Record: https://www.sciencedirect.com/science/article/pii/S0898122117305473
Manuscript_2d125cd1e89e9c095432816612ad64e2

Weakly compressible Lattice Boltzmann simulations of reacting flows with detailed thermo-chemical models

S.A. Hosseini[a,b,*], A. Eshghinejadfard[a], N. Darabiha[b], D. Thévenin[a]

[a] *Laboratory of Fluid Dynamics and Technical Flows, University of Magdeburg "Otto von Guericke", D-39106 Magdeburg, Germany*
[b] *Laboratoire EM2C, CNRS, CentraleSupélec, Université Paris-Saclay, 3 rue Joliot Curie, 91192, Gif-sur Yvette Cedex, France*

Abstract

Given the complex geometries usually found in practical applications, the Lattice Boltzmann (LB) method is becoming increasingly attractive for flow simulations. In addition to the simple treatment of intricate geometrical configurations, LB solvers can be implemented on very large parallel clusters with excellent scalability. However, reacting flows lead to additional challenges and have seldom been studied by LB methods. In this study, an in-house low Mach number Lattice Boltzmann solver, ALBORZ, has been extended to take into account multiple chemical components and reactions. For this purpose, the temperature and species each mass fraction field are modeled through separate distribution functions. The flow distribution function is assumed to be independent of temperature and species mass fractions, which is valid in the limit of weak density variations. In order to compute reaction terms as well as variable thermodynamic and transport properties, the LB code has been coupled to another library of our group, REGATH. In this manner, LB simulations with detailed chemical kinetics and thermo-chemical models become possible. Since the code is currently limited to weak density variation, its performance has been checked for a laminar premixed as well as non-premixed counter-flow Ozone/Air reacting flow, describing kinetics with 4 species and 18 elementary reactions. Comparisons of the obtained reacting flow structures with results from classical finite-difference simulations show excellent agreement.

Keywords: Lattice Boltzmann, Reacting flows, Multiple distribution function, Complex chemistry
2010 MSC: 00-01, 99-00

1. Introduction

Under practical conditions, reacting flows take place in systems with a complex geometry (gas turbine, burner, furnace...) and involve a large number of chemical species. In combustion for example, many consecutive and competing reactions between stable species and radicals occur. It is often of crucial importance to include detailed chemistry. However, due to limited computational resources, conventional numerical methods soon become impractical, since they lead to unacceptably long computational times. In the last decade, the Lattice Boltzmann (LB) Method has emerged as a promising alternative for simulating a variety of complex flows. Contrary to classical continuum-based formulations, probability distribution functions in a discretized phase-space are transported in physical space for LB. Though historically originating from the Lattice Gas Automata (LGA) [1], the Lattice Boltzmann equations have been later shown to be discretized forms of the Boltzmann transport equation [2, 3, 4]. A typical LGA model consists of identical particles colliding and propagating on either a two-dimensional hexagonal, or a four-dimensional, face-centered hypercube lattice, with either 0 or 1 particle per phase and physical space point [1, 5]. Lattice Boltzmann

*Corresponding author
Email address: seyed.hosseini@ovgu.de (S.A. Hosseini)

models on the other hand, deal with the collision and propagation of non-boolean distribution functions. Assuming the distribution function to be close to equilibrium, Higuera and Jimenez [6] linearized the collision operator in the LB transport equation. The use of the Bhatnagar-Gross-Krook (BGK) operator [7] was then suggested by several authors [8, 9], opening the door for many successful flow simulations based on LB [10, 11].

However, reacting flows lead to additional challenges and have seldom been implemented in LB codes [12], though the BGK-LB scheme has been shown to be in principle appropriate for modeling flows with reactions. Kang et al. [13] developed a LB model to simulate coupled flow and chemical dissolution for a system involving only two species. They then generalized the model to take into account precipitation [14, 15]. Yamamoto et al. [16] used a model based on the double distribution function formulation developed by He et al. [17] to simulate a one-dimensional propane flame, assuming a single reaction and constant density and thermo-physical properties. A number of other researchers have used the weakly compressible LB formulation for reacting flows to model combustion systems [18, 19].

As an alternative to a self-contained LB solver, Filippova and Hänel [20] have developed a hybrid finite difference/Lattice Boltzmann scheme to model dilatable combustion systems. Here, the fluid flow field was modeled through the classical, weakly compressible LB solver, while the temperature and species fields were handled using a standard finite-difference solver. Although this solution appears to be straightforward, it leads to complex coupling issues between two independent codes with very different structures, and can severely limit parallel scalability. An approach purely based on Lattice Boltzmann models would be more efficient, if it can take into account simultaneously thermal dilatation effects, complex multi-species kinetics and accurate thermochemical models as well as molecular diffusion.

A first attempt has been described in [21], relying on a modified equilibrium distribution function to incorporate an equation of state and a so-called particle characteristic temperature. This approach leads to variable lattice sound speed and hence – even in the case of fixed grid spacing – variable time step. Although dilatation effects can be taken into account with this technique, it does not handle detailed chemistry, nor variable thermodynamic and transport properties. These aspects are essential for an accurate description of combustion processes. Recently, Xu et al. [22] have proposed a compressible and dilatable lattice Boltzmann model for the flow and temperature fields. This model is based on another class of lattice Boltzmann formulations called multi-speed [23, 24, 25]. Such multi-velocity formulations – thanks to the larger number of velocities available – conserve the second-order moment of the distribution function and can therefore model density variations without needing any additional source term. Therefore when density, velocity and temperature fields are modeled through a single probability distribution function all of the macroscopic properties relax at a common rate. Xu et al. [22] overcame this issue by using a multiple relaxation time approach to model the effects of combustion on the flow and temperature fields; however, this is known to reduce noticeably computational efficiency. In [22], only the flow and temperature fields are investigated. Even more recently, Lin et al. [26] used the same multi-speed model, with a single relaxation time collision operator, to simulate a flow with two components. In their formulation, the chemical reaction was modeled through an additional BGK collision operator, and effects of heat production from an exothermic reaction on flow field were incorporated using Maxwell-Boltzmann's full equilibrium distribution function and the equipartition theorem. Although this approach has the advantage of modeling non-equilibrium effects, the use of the full Maxwell-Boltzmann equilibrium distribution function and multiple relaxation time collision operator along with the large number of discrete velocities negatively impacts computational efficiency.

None of the previously cited works took into account the variations of physicochemical properties due to temperature and chemical composition. However, changes of thermodynamic parameters and transport coefficients in space and time are of the utmost importance for many applications, such as combustion. In an effort toward describing such combustion systems with the LB method, the present article describes methods and numerical solutions that allow LB simulations of multi-species reacting flows with complex kinetics. At the same time, accurate models are used to describe varying thermodynamic and transport properties. All modifications are implemented in the in-house code ALBORZ [27], which already allows an efficient description of heat transfer processes [28] and can be used to solve flows in complex geometries [29]. The remaining challenge concerns the efficient description of mixing and reaction in a complex multi-species flow, as described in what follows. The present work, contrary to previous LB simulations involving multiple

Nomenclature

α	Lattice direction index
$\bar{c}_p$	Mixture-averaged specific heat capacity at constant pressure
$\bar{W}$	Mixture average molar mass
ΔH_i^0	Enthalpy change for reaction i
ΔS_i^0	Entropy change for reaction i
δ_t	Time-step
δ_x	Lattice spacing
$\dot{\omega}$	Heat release rate per unit volume
$\dot{\omega}_k$	Molar production rate per unit volume of the kth species
λ	Thermal conductivity
ν	Fluid kinematic viscosity
ρ	Fluid density
τ	Relaxation constant
τ_k	Relaxation constant of kth species mass fraction field
τ_T	Temperature field relaxation constant
$\vec{u}$	Fluid macroscopic velocity vector
$\vec{V}_k$	Diffusion velocity of the kth species
$\vec{x}$	Position vector in space
c	Lattice advection velocity
c_s	Lattice sound speed
D_k	Diffusion coefficient of the kth species
F_α	Temperature field distribution function
f_α	Flow field distribution function
$F_\alpha^{(eq)}$	Temperature field equilibrium distribution function
$f_\alpha^{(eq)}$	Flow field equilibrium distribution function
$g_{\alpha,k}$	Mass fraction field distribution function of the kth species
$g_{\alpha,k}^{(eq)}$	Mass fraction field equilibrium distribution function of the kth species
$g_{\alpha,k}^{*}$	Mass fraction field post-collision distribution function of the kth species
h_k	Total enthalpy of the k$^{\text{th}}$ species
$k, k^{'}$	Chemical species index
p	Thermodynamic pressure
s_k	Enthropy of the k$^{\text{th}}$ species
T	Temperature
t	Time
W_k	Molar mass of the kth species
X_k	Mole fraction of the kth species
Y_k	Mass fraction of kth species

species, implements variable viscosity, heat conductivity and species diffusion coefficients. This is necessary for a proper simulation of reacting flows and flames, since these properties vary strongly near reaction zones. In the context of the multiple distribution formulation, a distribution function is defined for each chemical species, for the temperature, and for the flow field. Modeling each of these variables with a different PDF allows for non-constant values of Prandtl, Lewis, and Schmidt numbers, while still considering a single relaxation time per equation. The evolution of all distribution functions – and hence their moments – is solved by the Lattice Boltzmann solver. All terms describing chemical kinetics (in particular production terms) as well as thermodynamic and transport properties are computed by coupling ALBORZ to a specific library, REGATH [30, 31, 32]. This library treats multi-species chemical reactions, variable thermodynamic and multi-component transport properties.

2. Lattice Boltzmann equations

In the context of the present study a weakly compressible 2-D square lattice BGK model has been used (D2Q9, [33]). The same grid structure and spacing is used for temperature and species fields.

2.1. Flow field

The flow field evolution is governed by the following equation:

$$f_\alpha(\vec{x}+\vec{c}_\alpha\delta_t,\vec{c}_\alpha,t+\delta_t)-f_\alpha(\vec{x},\vec{c}_\alpha,t)=-\frac{1}{\tau}\left(f_\alpha(\vec{x},\vec{c}_\alpha,t)-f_\alpha^{eq}(\vec{x},\vec{c}_\alpha,t)\right), \tag{1}$$

where $f_\alpha(\vec{x}+\vec{c}_\alpha\delta_t,\vec{c}_\alpha,t+\delta_t)$ is the discretized distribution function in a given direction α at a given time t and location $\vec{x}$, $f_\alpha^{eq}(\vec{x},\vec{c}_\alpha,t)$ is the equilibrium distribution function in the same direction and time, τ is the non-dimensional relaxation time and δ_t is the time-step. The distribution functions evolve in a square lattice structure with 9 discrete velocity vectors defined as:

$$\vec{c}_\alpha=(0,0) \qquad \text{for } \alpha=0, \tag{2}$$

$$\vec{c}_\alpha=\left(\cos\left[\frac{\alpha-1}{2}\pi\right],\sin\left[\frac{\alpha-1}{2}\pi\right]\right).c \qquad \text{for } \alpha=1\ldots4, \tag{3}$$

$$\vec{c}_\alpha=\left(\cos\left[\frac{(\alpha-5)\pi}{2}+\frac{\pi}{4}\right],\sin\left[\frac{(\alpha-5)\pi}{2}+\frac{\pi}{4}\right]\right).\sqrt{2}c \qquad \text{for } \alpha=5\ldots8, \tag{4}$$

where $c=\delta_x/\delta_t$ is known as the lattice advection velocity. The equilibrium distribution function is given by:

$$f_\alpha^{eq}\left(\vec{x},\vec{c}_\alpha,t\right)=w_\alpha\rho\left[1+\frac{1}{c_s^2}\vec{e}_\alpha.\vec{u}+\frac{1}{2c_s^4}(\vec{e}_\alpha.\vec{u})^2-\frac{1}{2c_s^2}\vec{u}.\vec{u}\right], \tag{5}$$

with $\vec{e}_\alpha$ the unit vector in direction α defined by $\vec{e}_\alpha=\vec{c}_\alpha/c_s$, where c_s is known as the lattice sound speed and defined by $c_s=c/\sqrt{3}$. The quantity w_α is the weight associated to the direction α, with:

$$w_\alpha=1/4 \qquad \text{for } \alpha=0, \tag{6}$$

$$w_\alpha=1/9 \qquad \text{for } \alpha=1\ldots4, \tag{7}$$

$$w_\alpha=1/36 \qquad \text{for } \alpha=5\ldots8. \tag{8}$$

The variable ρ is the weakly varying local fluid density. The density and macroscopic velocity $\vec{u}$, being zeroth- and first-order moments of the distribution function, are computed as:

$$\rho=\sum_{\alpha=0}^{8}f_\alpha, \tag{9}$$

$$\rho\vec{u}=\sum_{\alpha=0}^{8}f_\alpha\vec{c}_\alpha. \tag{10}$$

In this context, the non-dimensional relaxation time τ of Eq. (1) can be defined through a Chapman-Enskog expansion as:

$$\nu=\frac{2\tau-1}{2}c_s^2\delta_t. \tag{11}$$

Although ALBORZ has both SRT and MRT solvers for the flow field, only the SRT model has been used in the context of the present study to minimize computation times given the small Reynolds numbers of the studied test-cases.

2.2. Temperature and species fields

Following the double distribution formulation of He et al. [17], the temperature and species fields are modeled through separate distribution functions (F and g_k) evolving as [34]:

$$F_\alpha(\vec{x}+\vec{c}_\alpha\delta_t,\vec{c}_\alpha,t+\delta_t)-F_\alpha(\vec{x},\vec{c}_\alpha,t)=-\frac{1}{\tau_T}\left(F_\alpha(\vec{x},\vec{c}_\alpha,t)-F_\alpha^{eq}(\vec{x},\vec{c}_\alpha,t)\right)+w_\alpha\frac{\dot{\omega}\delta_t}{\bar{c}_p\rho T_{\text{ref}}}, \tag{12}$$

$$g_{k,\alpha}(\vec{x}+\vec{c}_\alpha\delta_t,\vec{c}_\alpha,t+\delta_t)-g_{k,\alpha}(\vec{x},\vec{c}_\alpha,t)=-\frac{1}{\tau_k}\left(g_{k,\alpha}(\vec{x},\vec{c}_\alpha,t)-g^{eq}_{k,\alpha}(\vec{x},\vec{c}_\alpha,t)\right)+w_\alpha\frac{\dot{\omega}_k W_k\delta_t}{\rho}, \tag{13}$$

with $k=1,...,N_{sp}$, considering a total number of N_{sp} species in the mixture. The last term appearing on the RHS, in both equations, is the chemical production rate per time step. The quantity $\dot{\omega}$ represents the production rate due to heat release per unit volume, $\dot{\omega}_k$ and W_k respectively correspond to the k^{th} species molar production rate per unit volume and molar mass. The equilibrium distribution functions are defined as:

$$F^{eq}_\alpha(\vec{x},\vec{c}_\alpha,t)=w_\alpha T\left[1+\frac{1}{c_s^2}\vec{e}_\alpha.\vec{u}\right], \tag{14}$$

$$g^{eq}_{k,\alpha}(\vec{x},\vec{c}_\alpha,t)=w_\alpha Y_k\left[1+\frac{1}{c_s^2}\vec{e}_\alpha.\vec{u}\right]. \tag{15}$$

Being limited to the first two terms of the Taylor expansion of the equilibrium distribution function, these are sometimes referred to as "linear" equilibrium distribution functions [34]. The relaxation coefficients can be related to macroscopic properties through a Chapman-Enskog analysis [35]:

$$\frac{\lambda}{\rho\bar{c_p}}=\frac{2\tau_T-1}{2}c_s^2\delta_t, \tag{16}$$

$$D_k=\frac{2\tau_k-1}{2}c_s^2\delta_t. \tag{17}$$

where both D_k and λ are respectively the k^{th} species diffusion coefficient and the mixture thermal conductivity. As with the flow field, macroscopic properties such as species mass fractions and temperature are then computed as:

$$T=\sum_{\alpha=0}^{8}F_\alpha, \tag{18}$$

$$Y_k=\sum_{\alpha=0}^{8}g_{k,\alpha}. \tag{19}$$

Summing up over all populations and using the Chapman-Enskog analysis, the following equation is recovered for the zeroth moment of the temperature distribution function:

$$\left(\frac{\partial}{\partial t}+\vec{\nabla}.\vec{u}\right)T-\vec{\nabla}.\left(\frac{\lambda}{\rho\bar{c_p}}\vec{\nabla}T\right)-\frac{1}{c_s^2}\vec{\nabla}.\left(\frac{\lambda}{\rho\bar{c_p}}\frac{\partial(\vec{u}T)}{\partial t}\right)=\frac{\dot{\omega}\delta_t}{\bar{c_p}\rho}. \tag{20}$$

Developing the second term on the LHS, one gets:

$$\left(\frac{\partial}{\partial t}+\vec{\nabla}.\vec{u}\right)T-\frac{1}{\rho\bar{c_p}}\vec{\nabla}.\left(\lambda\vec{\nabla}T\right)-\vec{\nabla}\left(\frac{1}{\rho\bar{c_p}}\right).\left(\lambda\vec{\nabla}T\right)-\frac{1}{c_s^2}\vec{\nabla}.\left(\frac{\lambda}{\rho\bar{c_p}}\frac{\partial(\vec{u}T)}{\partial t}\right)=\frac{\dot{\omega}\delta_t}{\bar{c_p}\rho}. \tag{21}$$

In the case of the species equations, a Chapman-Enskog development leads to the following macroscopic equation:

$$\left(\frac{\partial}{\partial t}+\vec{\nabla}.\vec{u}\right)Y_k-\vec{\nabla}.\left(D_k\vec{\nabla}Y_k\right)-\frac{1}{c_s^2}\vec{\nabla}.\left(D_k\frac{\partial(\vec{u}Y_k)}{\partial t}\right)=\frac{\dot{\omega}_k W_k\delta_t}{\rho}. \tag{22}$$

The second term on the LHS of Eq. (22) does not exactly correspond to the diffusion term appearing in the non-conservative form of the species transport equation. In order to get the correct form the following relation is used:

$$\vec{\nabla}.\left(D_k\vec{\nabla}Y_k\right)=\frac{\vec{\nabla}.\left(\rho D_k\vec{\nabla}Y_k\right)}{\rho}-\left(D_k\vec{\nabla}Y_k\right).\frac{\vec{\nabla}\rho}{\rho}. \tag{23}$$

The final form of the equation recovered by this model is:

$$\left(\frac{\partial}{\partial t}+\vec{\nabla}.\vec{u}\right)Y_k-\frac{\vec{\nabla}.\left(\rho D_k\vec{\nabla}Y_k\right)}{\rho}+\left(D_k\vec{\nabla}Y_k\right)\frac{\vec{\nabla}\rho}{\rho}-\frac{1}{c_s^2}\vec{\nabla}.\left(D_k\frac{\partial\vec{u}Y_k}{\partial t}\right)=\frac{\dot{\omega}_k W_k\delta_t}{\rho}. \tag{24}$$

In the limit of weak variations in density, the error due to the third and fourth terms on the LHS of Eq. (24) can be neglected. The fourth term can also be eliminated through the use of an additional force term defined as [36]:

$$F_\alpha=\left(1-\frac{1}{2\tau_k}\right)\frac{w_\alpha}{c_s^2}\vec{e}_\alpha.\frac{\partial(Y_k\vec{u})}{\partial t} \tag{25}$$

The time derivative can be evaluated through a simple finite-difference approximation; a first-order approximation is sufficient to recover second-order overall accuracy. The resulting equation corresponds to the macroscopic species transport equation with the Fick approximation for second-order accuracy in space. Owing to the deficiencies of the Fick approximation the scheme only conserves overall mass if all species have the same local diffusion coefficient, otherwise an additional correction term has to be included. A detailed Chapman-Enskog development of the passive scalar approach used in the context of this work is presented in Appendix A.

3. Multi-component thermodynamic and transport properties

3.1. Transport properties

For the transport of the k^{th} species in the mixture, the species conservation equations are expressed as follows:

$$\frac{\partial(\rho Y_k)}{\partial t}+\vec{\nabla}.\left[\rho(\vec{u}+\vec{V_k})Y_k\right]=\dot{\omega}_k W_k. \tag{26}$$

Here, Y_k is the local mass fraction of the k^{th} species, while $\vec{V_k}$ is the diffusion velocity, with:

$$\sum_{k=1}^{N_{sp}}Y_k\vec{V_k}=0. \tag{27}$$

Total mass conservation imposes:

$$\sum_{k=1}^{N_{sp}}\dot{\omega}_k W_k=0. \tag{28}$$

Retaining only one term in the Sonin polynomial expansion [37], the diffusion velocities are defined through the following system of equations [38] known as the Stephan-Maxwell diffusion equations:

$$\vec{\nabla}X_k=\sum_{k'=1}^{N_{sp}}\frac{X_kX_{k'}}{D_{pk'}}(\vec{V_{k'}}-\vec{V_k})+(Y_k-X_k)\frac{\vec{\nabla}p}{p}+\frac{\rho}{p}\sum_{k'=1}^{N_{sp}}Y_kY_{k'}(f_k-f_{k'}),\text{ for } k=1\dots N_{sp}, \tag{29}$$

in which the Soret effect has been neglected and $D_{k'k}=D_{kk'}$ is the binary diffusion coefficient of the k^{th} species into species $k^{'}$, p is the thermodynamic pressure, and X_k is the local mole fraction of the k^{th} species defined as:

$$X_k=\frac{Y_k\bar{W}}{W_k} \tag{30}$$

where the mixture molar mass $\bar{W}$ is computed as:

$$\bar{W}=\sum_k X_kW_k \tag{31}$$

The resolution of Eq. (29) to obtain $\vec{V}_k$ being very complex and time-consuming, simplified models are generally used instead. Supposing pressure gradient and external forces are negligible and retaining only first-order terms in the solution [37], $\vec{V}_k$ can be approximated with the formulation of Hirschfelder and Curtis, or alternatively with that of Fick, defined respectively as:

$$\vec{V}_k X_k = -D_k \vec{\nabla} X_k \text{ with } D_k = \frac{1 - Y_k}{\sum_{k' \neq k} X_{k'}/D_{k'k}}, \tag{32}$$

$$\text{or} \qquad \vec{V}_k Y_k = -D_k \vec{\nabla} Y_k \text{ with } D_k = \frac{1 - X_k}{\sum_{k' \neq k} X_{k'}/D_{k'k}}. \tag{33}$$

In the context of the present study, the local thermal conductivity is evaluated using a combination of averaging formula proposed by Burgoyne and Weinberg [39, 40]:

$$\lambda = \frac{1}{2} \sum_{k=1}^{N_{sp}} X_k \lambda_k + \left(\sum_{k=1}^{N_{sp}} \frac{X_k}{\lambda_k} \right)^{-1}, \tag{34}$$

where λ_k is the k^{th} species thermal conductivity. The mixture viscosity is computed using Wilke's semi-empirical formula [41], later modified by Bird et al. [42], and expressed as:

$$\mu = \sum_{k=1}^{N_{sp}} \frac{X_k \mu_k}{\sum_{k'=1}^{N_{sp}} X_p \Phi_{kk'}}, \tag{35}$$

with

$$\Phi_{k'k} = \frac{1}{\sqrt{8}} \left(1 + \frac{W_k}{W_{k'}} \right)^{-\frac{1}{2}} \left(1 + \left(\frac{\mu_k}{\mu_{k'}} \right)^{\frac{1}{2}} \left(\frac{W_{k'}}{W_k} \right)^{\frac{1}{4}} \right)^2, \tag{36}$$

where μ_k is the viscosity of the k^{th} species and μ represents the mixture viscosity.

3.2. Thermo-chemical properties

To get the thermo-chemical and transport properties, REGATH subroutines extract properties such as heat capacity using the NASA Chemical Equilibrium with Application (CEA) database as polynomial functions of order N of temperature:

$$\frac{C_{pk}}{R} = \sum_{n=1}^{N} a_{nk} T^{(n-1)}. \tag{37}$$

Here, R is the ideal gas constant. The specific heat capacity at constant pressure of the k^{th} species, and the mixture, are then expressed as follows:

$$c_{pk} = \frac{C_{pk}}{W_k}, \tag{38}$$

$$\bar{c}_p = \sum_{k=1}^{N_{sp}} c_{pk} Y_k. \tag{39}$$

The species production rate is one of the key components for reacting flow simulations with detailed chemistry. Considering a detailed chemical scheme involving N_{sp} species in I elementary reactions represented in the form:

$$\sum_{k=1}^{N_{sp}} \nu'_{ki} \chi_k \rightleftharpoons \sum_{k=1}^{N_{sp}} \nu''_{ki} \chi_k, \text{ for } i = 1 \dots I, \tag{40}$$

with $\nu_{ki}^{'}$ and $\nu_{ki}^{''}$ being balance coefficients, the production rate of the k^{th} species $\dot{\omega}_k$ is computed as:

$$\dot{\omega}_k = \sum_{i=1}^{I} \nu_{ki} q_i, \tag{41}$$

with:

$$\nu_{ki} = \nu_{ki}^{''} - \nu_{ki}^{'}. \tag{42}$$

The progress rate of reaction i, written q_i, reads:

$$q_i = k_{fi} \prod_{k=1}^{N_{sp}} [X_k]^{\nu_{ki}^{'}} - k_{ri} \prod_{k=1}^{N_{sp}} [X_k]^{\nu_{ki}^{''}}, \tag{43}$$

and involves the molar concentration of species k, written $[X_k]$. Finally, the reaction rate constants k_{fi} and k_{ri} are all expressed by an Arrhenius-type function. The forward rate is computed as:

$$k_{fi} = A_i T^{\beta_i} \exp\left(\frac{-E_i}{RT}\right), \tag{44}$$

with A_i the pre-exponential factor, β_i the temperature exponent and E_i the activation energy of reaction i. The reverse reaction rate k_{ri} is calculated from the equilibrium constant as:

$$k_{ri} = \frac{k_{fi}}{k_i^{eq}} \tag{45}$$

The equilibrium constant k_i^{eq} can be defined as [43]:

$$k_i^{eq} = \left(\frac{p_0}{RT}\right)^{\sum_{N_{sp}}^{k=1} \nu_{ki}} \exp\left(\frac{\Delta S_i^0}{R} - \frac{\Delta H_i^0}{RT}\right) \tag{46}$$

where p_0 =1 ba, ΔH_i^0 and ΔS_i^0 are the enthalpy and entropy changes for reaction i:

$$\Delta H_i^0 = \sum_{k=1}^{N_{sp}} \nu_{ki} W_k h_k(T) \tag{47}$$

$$\Delta S_i^0 = \sum_{k=1}^{N_{sp}} \nu_{ki} W_k s_k(T) \tag{48}$$

where s_k and h_k are the entropy and total enthalpy (accounting for sensible and chemical contributions) of the k^{th} species.

4. Code structure and algorithm

The new code is composed of two main computational tools: the main one is the Lattice Boltzmann solver ALBORZ, while all kinetic, thermodynamic and transport terms are computed with REGATH library. The Lattice Boltzmann solver can model the evolution of all distribution functions, but the system of equations is not closed: the relaxation coefficients and source terms need closure. REGATH provides these closures using an ensemble of subroutines, knowing all relevant local macroscopic properties such as density, velocity, mass fractions and temperature from LB solver. The structure of the resulting code is illustrated in Fig. 1.

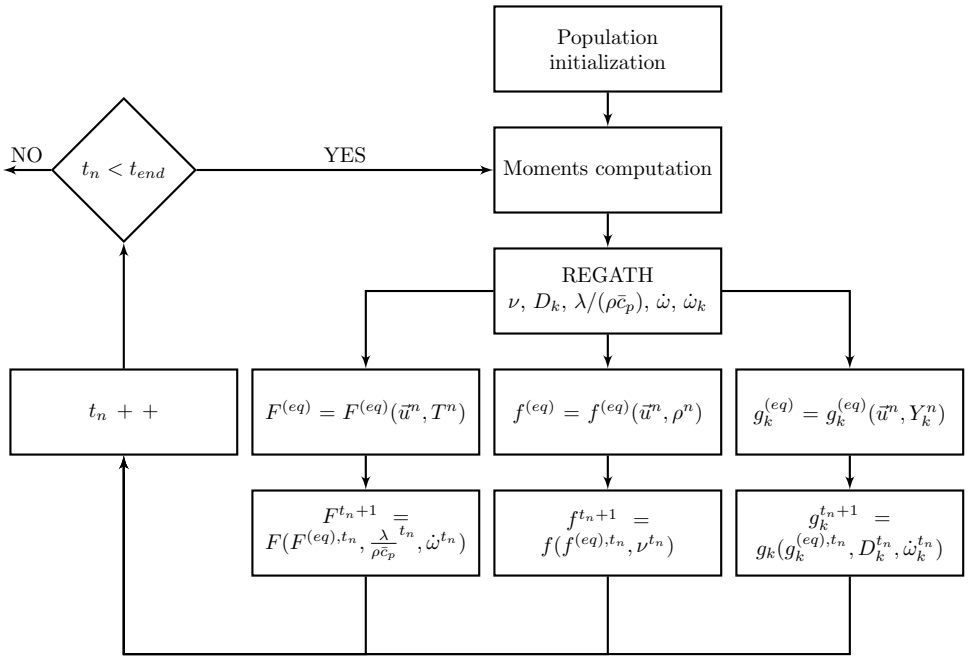

Figure 1: Coupled code structure between ALBORZ and REGATH

In a single time iteration, the distribution functions in the Lattice Boltzmann solver evolve using the thermodynamic and transport properties computed at the end of the previous iteration by REGATH. Looking back at Eqs. (1), (5) and (12–17), the mesoscopic fields rely on a number of parameters to evolve from a given time-step n to $n+1$. In order to model temperature and species convection, the macroscopic velocity from the flow field is needed. Similar to classical explicitly-coupled numerical methods the velocity is taken from the flow field at time step n. Diffusion terms in all fields (flow, temperature, and species) are controlled by their respective relaxation coefficients. The relaxation times –related to local viscosity, thermal conductivity, heat capacity and species diffusion coefficients– are computed using Eqs. (32–39). Similar to the velocity field, these parameters are explicitly coupled since they are computed using macrosopic values from time-step n. The source terms appearing in the PDF evolution equations are also evaluated based on macroscopic properties at time step n. Once the distribution functions have "collided and propagated", the new moments are computed, delivering density, velocity, temperature and mass fractions from their respective mesoscopic fields (Probability Distribution Functions) using Eqs. (9, 10,18) and (19). The mesoscopic fields are therefore all explicitly coupled through convection velocity, relaxation rates, and source terms. As previously mentioned, the flow field modifies the temperature and species field through convection as a first-order velocity term appearing in their equilibrium distribution function. The temperature PDF is affected by the species fields through two different channels: (1) The source term (heat production or consumption from chemical reactions) appearing in the mesoscopic evolution equation, and (2) mixture-averaged relaxation coefficient, which is a function of the mixture-averaged thermal conductivity. The species PDFs are affected by each other and the temperature field through the same two mechanisms. In the current model, the flow field PDF is only affected by the other fields through its relaxation time, related to mixture viscosity.

5. Computational setup: ozone/air reacting flow

In order to check the numerical procedure, two configurations involving ozone oxidation in air are considered: 1) a laminar premixed case, and 2) a counter-flow diffusion case. Both have been computed using the ALBORZ-REGATH coupled code described in the previous section. For comparison, a reference solution is obtained with a classical finite-difference solver, which is included as well in the REGATH package

(REGATH-1D). The details about the formulation of this solver are given in Appendix B –for the premixed case– and in Appendix C –for the counter-flow case. This means that the reference solution, based on the standard conservation equations for the continuum, is obtained using REGATH-1D as standalone code; while the LB solution is obtained by ALBORZ coupled with the corresponding REGATH libraries for kinetics, thermodynamics and transport.

All simulations with both codes rely on a detailed kinetic scheme taking into account 4 species (O, O_2, O_3 and N_2) and 18 elementary reaction steps, described by Ombrello et al. [44] and listed in Appendix D.

5.1. Properties of ozone/air reacting flow

As mentioned previously, the coupled code in its current state does not take into account any effect of compression or thermal dilatation. As a consequence, an ozone reacting flow has been retained, for which these effects are negligible. Indeed, the reference solution from REGATH-1D shows that temperature and density variations are very small. As shown in Fig. 2, the variations of temperature and density for a typical configuration amount to 0.9 K and 10^{-3} kg.m^{-3} respectively, which means in both cases a relative difference below 0.2%. Both effects can therefore be neglected.

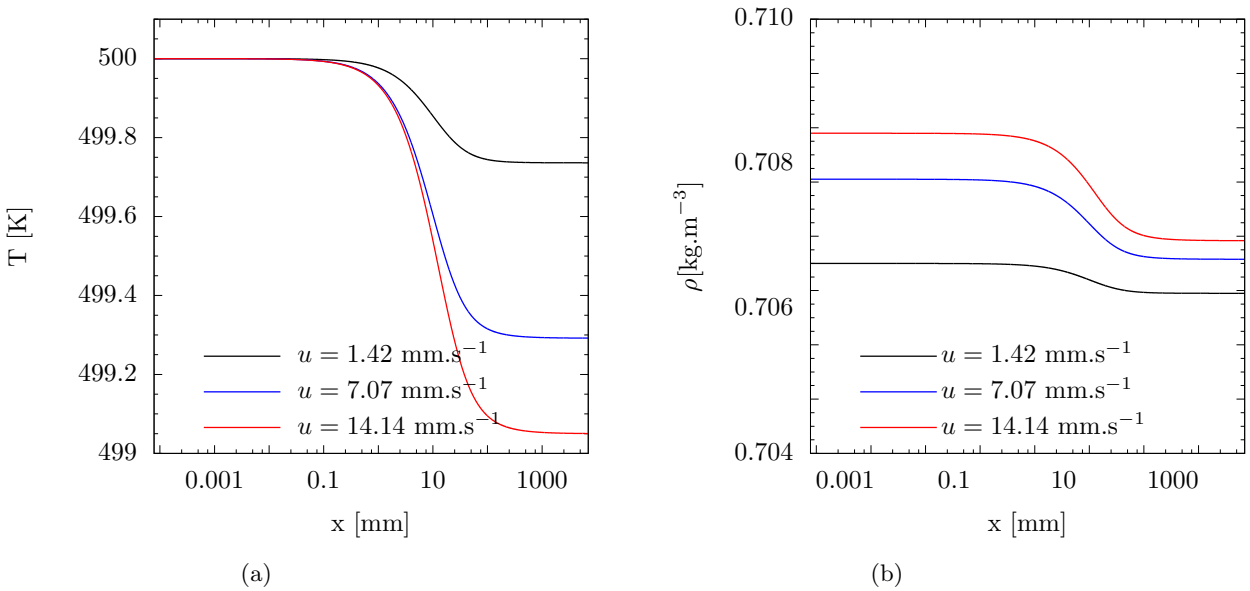

Figure 2: Reference (a) temperature and (b) density solution for ozone/air reacting flow, density and temperature obtained with REGATH-1D (note that the vertical scales are very small)

5.2. Geometrical configuration

Since laminar conditions are considered, one-dimensional simulations are sufficient for the premixed reacting flow.

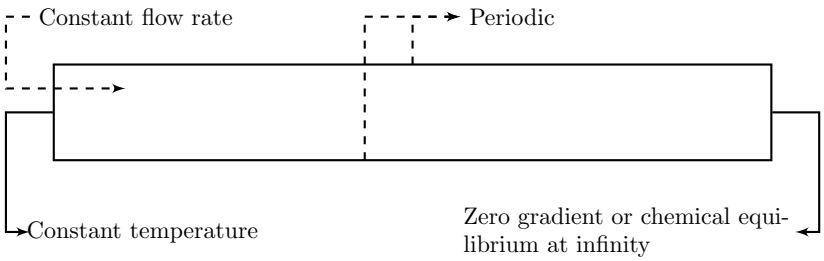

Figure 3: Geometrical configuration and boundary conditions for the first test-case (ozone/air premixed reacting jet)

The geometrical configuration and boundary conditions of this test-case are represented in Fig. 3. Since the lattice structure used in the code is at least 2-D, periodic boundary conditions were applied to the $y-$boundaries in order to model a 1-D configuration. The fresh gas entering the simulation domain at the left is assumed to be at a constant temperature of 500 K, with a constant macroscopic velocity. Its composition, corresponding to the term on the RHS of Eqs.(49) and (B.4), is given in Table 1.

species	O	O_2	O_3	N_2
$Y_{k,0}$	0.000	0.228	0.020	0.752

Table 1: Imposed chemical composition of the fresh gas

Preliminary studies using the finite difference solver have shown that the flow reaches chemical equilibrium at a distance of approximately 7m from the inlet while displaying high gradients near the inlet. In order to capture both scales while keeping acceptable computational cost, the simulation was performed using variable-size grids. The grids were dilated in the horizontal direction through an off-lattice propagation strategy proposed by Luo et al. All details can be found in [45]. A typical grid generated through this approach and used in the context of the present study is illustrated in Fig. 4.

Figure 4: Grid generated in the context of the off-lattice propagation approach

In order to keep the spatial order of accuracy of the method, and to limit numerical diffusion, quadratic functions were used for the interpolation step.

The second test-case (counter-flow non-premixed configuration) consists of two inflows in opposite direction facing each other, and two constant-pressure outlet boundaries. The geometrical configuration along with boundary conditions are shown in Fig. 5.

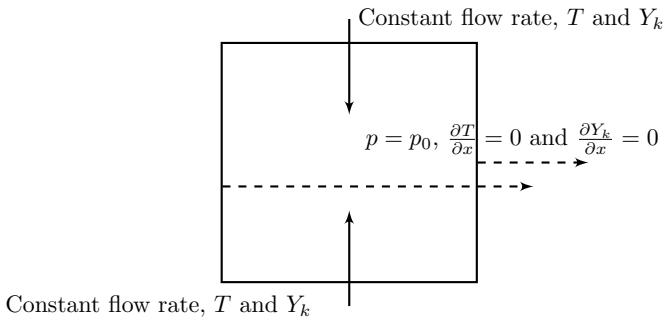

Figure 5: Geometrical configuration and boundary conditions for the second test-case (counter-flow non-premixed ozone reacting flow)

The simulation domain consists of a 4 mm by 4mm square rectangular area. At both inlets constant velocity, constant temperature and composition boundary conditions were applied while the outlets are modeled using constant pressure and zero-gradient temperature and mass fraction conditions. Corresponding values are listed in Table 2.

parameter	Y_{O}	$Y_{\mathrm{O_2}}$	$Y_{\mathrm{O_3}}$	$Y_{\mathrm{N_2}}$	T [K]	u_0 [m/s]
Inlet 1	0.000	0.233	0.000	0.767	300	0.3(0.5)
Inlet 2	0.000	0.000	0.233	0.767	300	0.3(0.5)

Table 2: Counter-flow configuration inlet composition and temperatures

Just as for the premixed configuration, 2 different inlet velocities (0.3 and 0.5 m/s) have been considered.

5.3. Boundary and initial conditions

Standard LB boundary conditions have been applied to the flow fields: In the case of the premixed reacting flow Constant density and velocity at the entrance (left) using Zou and He's formulation [46], zero-gradient at the outlet, and periodic along the horizontal boundaries. Equations based on the half-way anti-bounce-back model, have been used to impose a constant temperature at the inlet. For the species mass fractions, a modified version of the previously mentioned boundary condition has been developed and applied, replacing the pure Dirichlet boundary condition (imposed value) by a Robin-type boundary condition in order to model burner-stabilized cases (see Eq. (B.4)). For this purpose, the constant species flux at the inlet is expressed through the following equation:

$$\left(-D_k \frac{\vec{u}}{|\vec{u}|}.\vec{\nabla} Y_k + \vec{u} Y_k\right)\Big|_{inlet} = \vec{u} Y_{k,0}, \tag{49}$$

where Y_k is the local mass fraction of the k^{th} species, while $Y_{k,0}$ is the fresh gas mass fraction of the same species from Table 1. The quantity $\bar{W}$ is the molar mass of the local mixture. In a 1-D configuration, Eq. (49) can be approximated in discrete form as:

$$Y_{k,1} = \frac{u Y_{k,0} + \frac{D_k Y_{k,2}}{\delta_x}}{\frac{D_k}{\delta_x} + u}, \tag{50}$$

in which $Y_{k,1}$ and $Y_{k,2}$ are the mass fractions at the first (inlet boundary) and second grid points. This value was enforced at the boundary through a simple half-way anti-bounce-back formulation[47]:

$$g_{k,\alpha} = (w_\alpha + w_{\bar{\alpha}}) Y_{k,1} - g^*_{k,\bar{\alpha}} \tag{51}$$

where $g^*_{k,\bar{\alpha}}$ is the post-collision distribution function in the opposite direction of α. For the counter-flow configuration, Zou and He's formulation was used in order to impose the constant inlet velocity and constant pressure at the outlet, as for the first test-case. Constant temperature and flow composition at the inlets were applied using the anti-bounce-back approach. The simulations were initialized with constant density and temperature, and zero velocity everywhere. At initialization, the simulation domain only contains the non-reacting nitrogen species, N_2. The PDFs were initialized using the Equilibrium Distribution Functions corresponding to the previously mentioned macroscopic values.

6. Results and Discussion

In order to account for characteristic times of ozone chemistry, time steps of the order of 10 μs are needed (which is indeed relatively long for most combustion applications). LB simulations usually fail to converge for relaxation constants τ too close to 0.5 [48] and larger values tend the introduce additional numerical diffusion in the system. The non-dimensional velocity must also be kept small –usually below 0.1– in order to minimize the so-called compressibility error in the flow field. Taking these factors into consideration and keeping in mind the characteristic scales of the flow, the minimum –near the inlet– and maximum –near the outlet– cell lengths in the domain were set respectively to 5×10^{-5} m and 5×10^{-2} m in the premixed case. For the counter-flow configuration, the simulations were performed on a uniform grid of size 1×10^{-5} m.

6.1. Premixed reacting flow

In order to show the general applicability of the developed computational procedure, the impact of the inflow velocity on the obtained flame structure has been checked for three different cases in a realistic range: $u = 0.141$, 0.707 and 1.41 cm/s. The obtained results are displayed in Figs. 6 – 8.

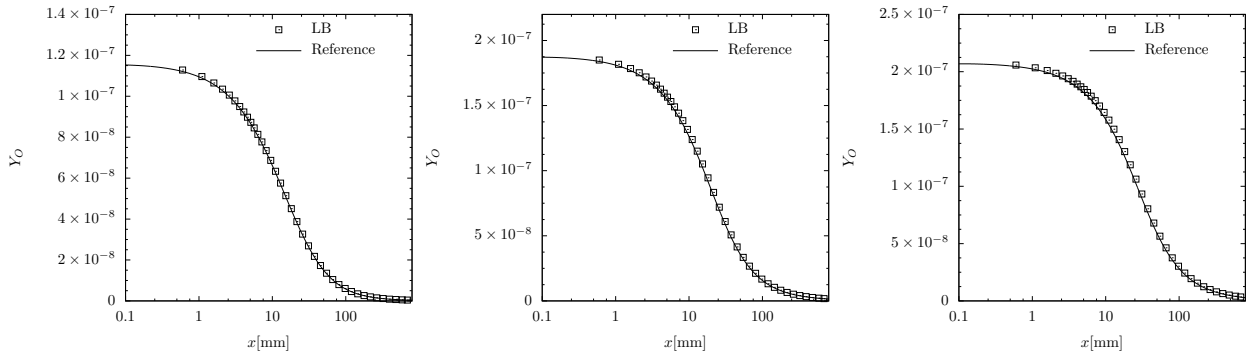

Figure 6: O radical mass fraction profile for three inlet velocities: (a) $u = 0.1414$ cm.s^{-1}, (b) $u = 0.707$ cm.s^{-1} and (c) $u = 1.414$ cm.s^{-1}

As the inlet velocity goes up from $u = 0.1414$ cm.s^{-1} to $u = 1.414$ cm.s^{-1}, Y_O increases at inlet while the flame length increases. This effect is illustrated in Fig. 6.

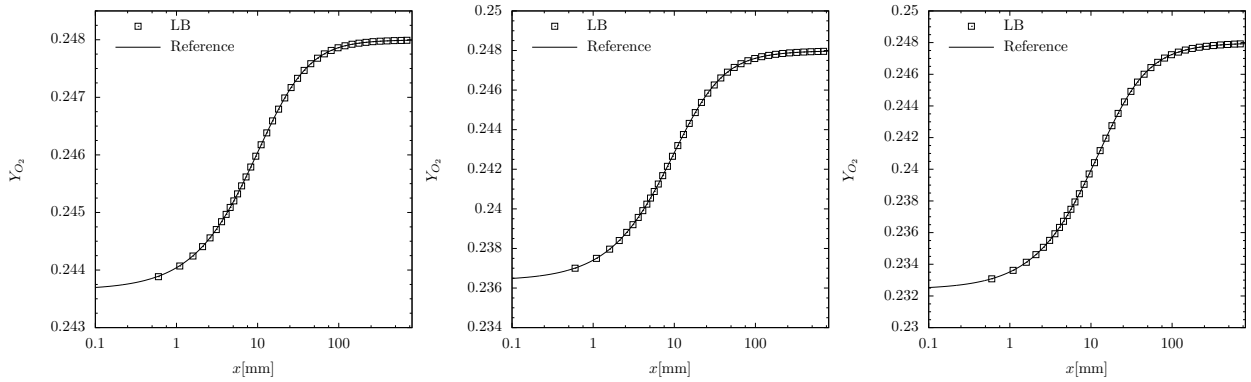

(a) (b) (c)

Figure 7: O_2 mass fraction profile for three inlet velocities: (a) $u = 0.1414$ cm.s^{-1}, (b) $u = 0.707$ cm.s^{-1} and (c) $u = 1.414$ cm.s^{-1}

According to Fig. 8 the chemical time-scale being much smaller than the flow time-scale at the inlet, O_3 dissociates into O and O_2. As the inlet velocity increases, the flow time-scale decreases pushing the inlet mass fractions closer to the fresh gas composition. For example, at $u = 0.1414$ cm.s^{-1}, $Y_{O_2}^{inlet} = 0.2437$ while as mentioned in Table 1, $Y_{O_2}^{fresh} = 0.228$. At higher inlet velocity, it goes down and reaches $Y_{O_2}^{fresh} = 0.2324$.

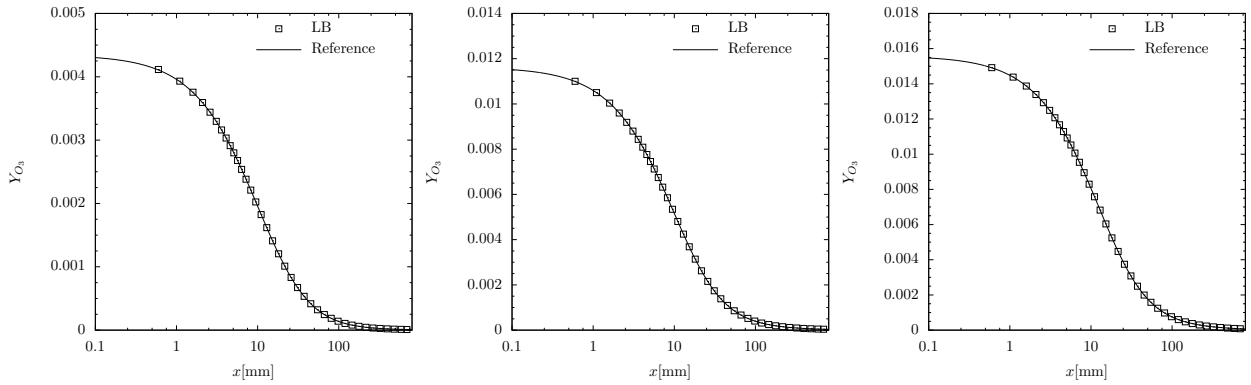

(a) (b) (c)

Figure 8: O_3 mass fraction profile for three inlet velocities: (a) $u = 0.1414$ cm.s^{-1}, (b) $u = 0.707$ cm.s^{-1} and (c) $u = 1.414$ cm.s^{-1}

195 As obvious from Figs. 6 to 8 the developed LB procedure reproduces accurately the reference results for all three inflow velocities.

6.2. Counter-current reacting flow

The simulations presented in this section were performed on a 400×400 grid. The overall structure of the velocity field along with the velocity profile on the vertical centerline are represented in Fig 9.

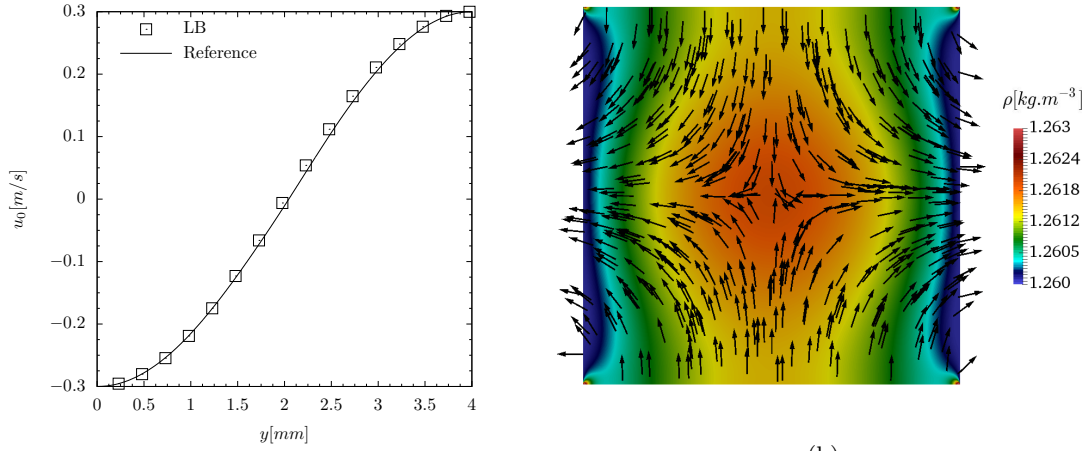

(a) (b)

Figure 9: (a) Velocity profile along the vertical centerline and (b) overall flow structure for the counter-flow case with inlet velocity of 0.3 m/s and mixture temperature of 300 K

The velocity profile obtained using the LB solver agrees very well with the one-dimensional reference solution from REGATH. This good agreement is observed for both inlet velocities considered in the study. It should be noted that the REGATH code uses a self-similarity approximation and gives only the solution in the vicinity of the jet axis.

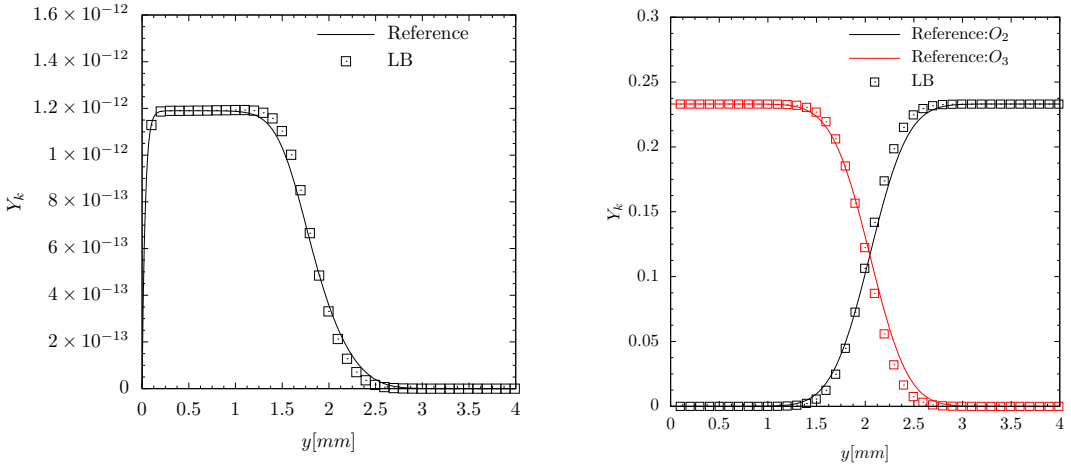

(a) (b)

Figure 10: Mass fraction profiles of (a) O, (b) O_2 and O_3 along the vertical centerline for u_0=0.3 m/s and T=300 K

As shown in Fig. 10, a small portion of O_3 dissociates into O and O_2 immediately after the inlet. The mixture rapidly reaches chemical equilibrium as Y_O increases to a threshold value of 1.2×10^{-12}. A similar behavior is observed for the cases with an inlet velocity of 0.5 m/s. The results of this configuration are illustrated in Fig. 11.

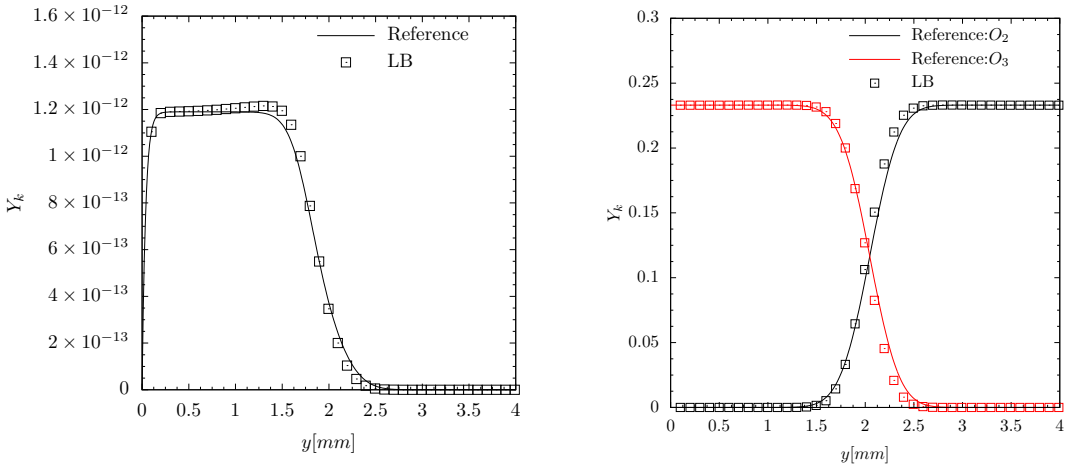

(a) (b)

Figure 11: Mass fraction profiles of (a) O, (b) O_2 and O_3 on the vertical centerline for u_0=0.5 m/s and T=300 K

In both cases, the LB solver is able to accurately reproduces the steady-state reference solution of REGATH.

6.3. Computational performance

A low computational time is one of the major advantages of LB solvers. In the present case, it is impossible to compare the overall computational times, since the reference, finite-difference solver REGATH only computes the steady-state solution, while LB inherently delivers the time-dependent solution. Still, the computational time needed for each iteration can be compared for both codes, using the same number of grid points. The results listed in Table 3 have been obtained on a single core of an i7 processor clocked at 2.3GHz. For the same number of grid points, the Lattice Boltzmann solver is approximately 6 times

	LB	reference (finite-difference)
computational time per iteration	0.165 s	1.0 s

Table 3: Comparison of computational time per iteration for 9000 grid points in space

faster per iteration than the finite-difference code, REGATH-1D. Considering additionally that LB solvers are known to scale much better in parallel (both for CPU and GPU), the motivation for developing Lattice Boltzmann models for complex applications involving reacting flows is clear.

7. Conclusions

A Lattice Boltzmann code, capable of handling an arbitrary number of species and reactions and taking into account multicomponent thermodynamic and transport properties has been successfully developed. The LB solver is based on the multiple distribution formulation, a passive scalar approach and uses a single relaxation time BGK collision operator. As such, it is able to handle variable Prandtl, Schmidt and Lewis numbers using the same collision operator and without much complication, at the difference of multi-velocity models.

An ozone/air reacting flow involving four species and 18 reactions has been computed with the resulting solver. After implementing a variable-sized grid in the solver, the LB results show excellent agreement compared to a classical reference solution obtained by finite differences, with a computational time per iteration about 6 times shorter.

In order to be able to model a broader range of exothermic reaction processes, the diffusion velocity correction and thermal dilatation must now be taken into account. For this purpose, an equation of state must be enforced through the use of a source term in the Lattice Boltzmann formulation. This is the subject of our current work and would open the door for LB simulations of combustion systems, and in particular of unsteady flames in complex geometries.

Acknowledgments

This work was supported by the European Regional Development Fund (ERDF/ EFRE) within the Research Center Dynamic Systems (CDS).

References

[1] U. Frisch, B. Hasslacher, Y. Pomeau, Lattice-gas automata for the Navier-Stokes equation, Physical Review Letters 56 (14) (1986) 1505.

[2] X. He, L.-S. Luo, A priori derivation of the Lattice Boltzmann equation, Physical Review E 55 (6) (1997) R6333.

[3] X. He, L.-S. Luo, Theory of the Lattice Boltzmann method: From the Boltzmann equation to the Lattice Boltzmann equation, Physical Review E 56 (6) (1997) 6811.

[4] T. Abe, Derivation of the Lattice Boltzmann method by means of the discrete ordinate method for the Boltzmann equation, Journal of Computational Physics 131 (1) (1997) 241–246.

[5] U. Frisch, D. dHumieres, B. Hasslacher, P. Lallemand, Y. Pomeau, J.-P. Rivet, Lattice gas hydrodynamics in two and three dimensions, Complex Systems 1 (4) (1987) 649–707.

[6] F. Higuera, J. Jiménez, Boltzmann approach to Lattice gas simulations, Europhysics Letters 9 (7) (1989) 663.

[7] P. L. Bhatnagar, E. P. Gross, M. Krook, A model for collision processes in gases. I: Small amplitude processes in charged and neutral one-component systems, Physical Review 94 (3) (1954) 511.

[8] S. Chen, H. Chen, D. Martnez, W. Matthaeus, Lattice Boltzmann model for simulation of magnetohydrodynamics, Physical Review Letters 67 (27) (1991) 3776.

[9] Y. H. Qian, Lattice gas and Lattice kinetic theory applied to the Navier-Stokes equations, Ph.D. thesis, Université Pierre et Marie Curie (1990).

[10] S. H. Kim, H. Pitsch, On the Lattice Boltzmann method for multiphase flows with large density ratios, Journal of Computational Physics 303 (2015) 19–27.

[11] H. Liu, Y. Ding, H. Wang, J. Zhang, Lattice Boltzmann method for the age concentration equation in shallow water, Journal of Computational Physics 299 (2015) 613–629.

[12] S. Ayodele, F. Varnik, D. Raabe, Lattice Boltzmann study of pattern formation in reaction-diffusion systems, Physical Review E 83 (1) (2011) 016702.

[13] Q. Kang, D. Zhang, S. Chen, X. He, Lattice Boltzmann simulation of chemical dissolution in porous media, Physical Review E 65 (3) (2002) 036318.

[14] Q. Kang, D. Zhang, S. Chen, Simulation of dissolution and precipitation in porous media, Journal of Geophysical Research: Solid Earth 108 (B10) (2003) 2505.

[15] Q. Kang, P. C. Lichtner, D. Zhang, An improved Lattice Boltzmann model for multicomponent reactive transport in porous media at the pore scale, Water Resources Research 43 (12) (2007) 14.

[16] K. Yamamoto, X. He, G. D. Doolen, Simulation of combustion field with Lattice Boltzmann method, Journal of Statistical Physics 107 (1-2) (2002) 367–383.

[17] X. He, S. Chen, G. D. Doolen, A novel thermal model for the Lattice Boltzmann method in incompressible limit, Journal of Computational Physics 146 (1) (1998) 282–300.

[18] H. Yu, L.-S. Luo, S. S. Girimaji, Scalar mixing and chemical reaction simulations using Lattice Boltzmann method, International Journal of Computational Engineering Science 3 (01) (2002) 73–87.

[19] E. Chiavazzo, I. V. Karlin, A. N. Gorban, K. Boulouchos, Combustion simulation via Lattice Boltzmann and reduced chemical kinetics, Journal of Statistical Mechanics: Theory and Experiment 2009 (06) (2009) P06013.

[20] O. Filippova, D. Hänel, A novel Lattice BGK approach for low mach number combustion, Journal of Computational Physics 158 (2) (2000) 139–160.

[21] S. Chen, Z. Liu, C. Zhang, Z. He, Z. Tian, B. Shi, C. Zheng, A novel coupled Lattice Boltzmann model for low Mach number combustion simulation, Applied Mathematics and Computation 193 (1) (2007) 266–284.

[22] A. Xu, C. Lin, G. Zhang, Y. Li, Multiple-relaxation-time Lattice Boltzmann kinetic model for combustion, Physical Review E 91 (4) (2015) 043306.

[23] F. J. Alexander, S. Chen, J. Sterling, Lattice Boltzmann thermohydrodynamics, Physical Review E 47 (4) (1993) R2249.

[24] G. R. McNamara, A. L. Garcia, B. J. Alder, Stabilization of thermal Lattice Boltzmann models, Journal of Statistical Physics 81 (1-2) (1995) 395–408.

[25] Y. Chen, H. Ohashi, M. Akiyama, Heat transfer in Lattice BGK modeled fluid, Journal of Statistical Physics 81 (1-2) (1995) 71–85.

[26] C. Lin, A. Xu, G. Zhang, Y. Li, Double-distribution-function discrete Boltzmann model for combustion, Combustion and Flame 164 (2016) 137–151.

[27] A. Eshghinejadfard, A. Abdelsamie, G. Janiga, D. Thévenin, Direct-forcing immersed boundary Lattice Boltzmann simulation of particle/fluid interactions for spherical and non-spherical particles, Particuology 25 (2016) 93–103.

[28] A. Eshghinejadfard, D. Thévenin, Numerical simulation of heat transfer in particulate flows using a thermal immersed boundary Lattice Boltzmann method, International Journal of Heat and Fluid Flow 60 (2016) 31–46.

[29] A. Eshghinejadfard, L. Daróczy, G. Janiga, D. Thévenin, Calculation of the permeability in porous media using the Lattice Boltzmann method, International Journal of Heat and Fluid Flow.

[30] N. Darabiha, REGATH: Thermodynamic, chemical and transport properties computation code, submitted to the French National Center for Scientific Research(CNRS) (2016).

[31] B. Franzelli, B. Fiorina, N. Darabiha, A tabulated chemistry method for spray combustion, Proceedings of the Combustion Institute 34 (1) (2013) 1659–1666.

[32] S. Candel, T. Schmitt, N. Darabiha, Progress in transcritical combustion: experimentation, modeling and simulation, Proceedings of 23rd ICDERS, Irvine USA (2011) 27.

[33] X. He, L.-S. Luo, Lattice Boltzmann model for the incompressible Navier-Stokes equation, Journal of Statistical Physics 88 (3-4) (1997) 927–944.

[34] Q. Li, Z. Chai, B. Shi, Lattice boltzmann model for a class of convection–diffusion equations with variable coefficients, Computers & Mathematics with Applications 70 (4) (2015) 548–561.
[35] B. Shi, Z. Guo, Lattice boltzmann simulation of some nonlinear convection–diffusion equations, Computers & Mathematics with Applications 61 (12) (2011) 3443–3452.
[36] B. Chopard, J. Falcone, J. Latt, The lattice boltzmann advection-diffusion model revisited, The European Physical Journal-Special Topics 171 (1) (2009) 245–249.
[37] V. Giovangigli, Convergent iterative methods for multicomponent diffusion, Impact of Computing in Science and Engineering 3 (3) (1991) 244–276.
[38] T. Poinsot, D. Veynante, Theoretical and numerical combustion, RT Edwards Inc., 2005.
[39] S. Mathur, P. Tondon, S. Saxena, Thermal conductivity of binary, ternary and quaternary mixtures of rare gases, Molecular Physics 12 (6) (1967) 569–579.
[40] J. Burgoyne, F. Weinberg, A method of analysis of a plane combustion wave, in: International Symposium on Combustion, Vol. 4, Elsevier, 1953, pp. 294–302.
[41] C. Wilke, A viscosity equation for gas mixtures, The Journal of Chemical Physics 18 (4) (1950) 517–519.
[42] R. Bird, W. Stewart, E. Lightfoot, Transport Phenomena, John Wiley & Sons, New York, 1960.
[43] K. K. Kuo, Principles of combustion, Wiley, 1986.
[44] T. Ombrello, S. H. Won, Y. Ju, S. Williams, Flame propagation enhancement by plasma excitation of oxygen. Part I: Effects of O_3, Combustion and Flame 157 (10) (2010) 1906–1915.
[45] X. He, L.-S. Luo, M. Dembo, Some progress in Lattice Boltzmann method. part i. nonuniform mesh grids, Journal of Computational Physics 129 (2) (1996) 357–363.
[46] Q. Zou, X. He, On pressure and velocity boundary conditions for the Lattice Boltzmann BGK model, Physics of Fluids 9 (6) (1997) 1591–1598.
[47] T. Zhang, B. Shi, Z. Guo, Z. Chai, J. Lu, General bounce-back scheme for concentration boundary condition in the lattice-boltzmann method, Physical Review E 85 (1) (2012) 016701.
[48] Y. Qian, D. d'Humières, P. Lallemand, Lattice BGK models for Navier-Stokes equation, Europhysics Letters 17 (6) (1992) 479.
[49] J. F. Grcar, R. J. Kee, M. D. Smooke, J. A. Miller, A hybrid newton/time-integration procedure for the solution of steady, laminar, one-dimensional, premixed flames, in: International Symposium on Combustion, Vol. 21, Elsevier, 1988, pp. 1773–1782.
[50] M. Smooke, P. Lin, J. Lam, M. Long, Computational and experimental study of a laminar axisymmetric methane-air diffusion flame, in: International Symposium on Combustion, Vol. 23, Elsevier, 1991, pp. 575–582.
[51] N. Darabiha, S. Candel, The influence of the temperature on extinction and ignition limits of strained hydrogen-air diffusion flames, Combustion science and technology 86 (1-6) (1992) 67–85.
[52] N. Darabiha, Transient behaviour of laminar counterflow hydrogen-air diffusion flames with complex chemistry, Combustion science and technology 86 (1-6) (1992) 163–181.
[53] B. Fiorina, O. Gicquel, L. Vervisch, S. Carpentier, N. Darabiha, Approximating the chemical structure of partially premixed and diffusion counterflow flames using FPI flamelet tabulation, Combustion and flame 140 (3) (2005) 147–160.

Appendix A. Chapman-Enskog Analysis of the D2Q9 Passive Scalar Transport scheme

An asymptotic analysis of the following evolution equation is to be made:

$$\phi_\alpha(\vec{x}+\vec{c}_\alpha,\vec{c}_\alpha,t+1)-\phi_\alpha(\vec{x},\vec{c}_\alpha,t)=-\frac{1}{\tau}\left(\phi_\alpha(\vec{x},\vec{c}_\alpha,t)-\phi_\alpha^{(eq)}(\vec{x},\vec{c}_\alpha,t)\right) \tag{A.1}$$

where ϕ_α is the distribution function corresponding to the passive scalar being transported. For the passive scalar transport approach, only zeroth-order moments need to be conserved. Therefore, we define the equilibrium distribution function as:

$$\phi_\alpha^{eq}(\vec{x},\vec{c}_\alpha,t)=w_\alpha\Xi\left[1+\frac{1}{c_s^2}\vec{e}_\alpha.\vec{u}\right], \tag{A.2}$$

where Ξ is the passive scalar being transported and $\vec{u}$ is the macroscopic velocity computed as the first moment of the flow field distribution function. To recover the macroscopic transport equation, the following multi-scale expansions need to be made:

$$\phi_\alpha=\phi_\alpha^{(0)}+\epsilon\phi_\alpha^{(1)}+\epsilon^2\phi_\alpha^{(2)}+\mathcal{O}(\epsilon^3) \tag{A.3}$$

$$\partial_t=\epsilon\partial t^{(1)}+\epsilon^2\partial t^{(2)}+\mathcal{O}(\epsilon^3) \tag{A.4}$$

$$\vec{\nabla}=\epsilon\vec{\nabla}^{(1)}+\epsilon^2\vec{\nabla}^{(2)}+\mathcal{O}(\epsilon^3) \tag{A.5}$$

with the following properties:

$$\sum_\alpha\phi_\alpha^{(0)}=\Xi \tag{A.6}$$

$$\sum_\alpha\phi_\alpha^{(i)}=0 \text{ for } i\neq 0 \tag{A.7}$$

Notice that the corresponding assumptions for the first moment of the distribution function have been dropped. This is due to the fact that we are only conserving zeroth-order moments and therefore can not impose these conditions on the first-order moment. Applying the Taylor expansion to the LHS of the LB equation up to second order, we get:

$$\phi_\alpha(\vec{x}+\vec{c}_\alpha,\vec{c}_\alpha,t+1)-\phi_\alpha(\vec{x},\vec{c}_\alpha,t)=\partial_t\phi_\alpha+\vec{c}_\alpha.\vec{\nabla}\phi_\alpha+\frac{1}{2}\left(\partial_t+\vec{c}_\alpha.\vec{\nabla}\right)^2\phi_\alpha \tag{A.8}$$

Putting these multi-scale expansions into Eq. (A.1) we get:

$$\begin{aligned}&\left(\epsilon\partial t^{(1)}+\epsilon^2\partial t^{(2)}+\epsilon\vec{c}_\alpha.\vec{\nabla}^{(1)}+\epsilon^2\vec{c}_\alpha.\vec{\nabla}^{(2)}\right)\left(\phi_\alpha^{(0)}+\epsilon\phi_\alpha^{(1)}+\epsilon^2\phi_\alpha^{(2)}\right)+\\&\frac{1}{2}\left(\epsilon\partial t^{(1)}+\epsilon^2\partial t^{(2)}+\epsilon\vec{c}_\alpha.\vec{\nabla}^{(1)}+\epsilon^2\vec{c}_\alpha.\vec{\nabla}^{(2)}\right)^2\left(\phi_\alpha^{(0)}+\epsilon\phi_\alpha^{(1)}+\epsilon^2\phi_\alpha^{(2)}\right)=-\frac{1}{\tau}\left(\epsilon\phi_\alpha^{(1)}+\epsilon^2\phi_\alpha^{(2)}\right)\end{aligned} \tag{A.9}$$

Separating terms of different order in ϵ into different equations, for the first- and second-order equations we get:

$$\left(\partial t^{(1)}+\vec{c}_\alpha.\vec{\nabla}^{(1)}\right)\phi_\alpha^{(0)}=-\frac{\phi_\alpha^{(1)}}{\tau} \tag{A.10}$$

$$\left(\partial t^{(1)}+\vec{c}_\alpha.\vec{\nabla}^{(1)}\right)\phi_\alpha^{(1)}+\left(\partial t^{(2)}+\vec{c}_\alpha.\vec{\nabla}^{(2)}\right)\phi_\alpha^{(0)}+\frac{1}{2}\left(\partial t^{(1)}+\vec{c}_\alpha.\vec{\nabla}^{(1)}\right)^2\phi_\alpha^{(0)}=-\frac{\phi_\alpha^{(2)}}{\tau} \tag{A.11}$$

Computing the zeroth moment of Eq. (A.10):

$$\left(\partial t^{(1)}+\vec{\nabla}^{(1)}.\vec{u}\right)\Xi=0 \tag{A.12}$$

Doing the same for Eq. (A.11):

$$\left(\partial t^{(2)} + \vec{\nabla}^{(2)}.\vec{u}\right)\Xi + \left(\partial t^{(1)} + \vec{c}_\alpha.\vec{\nabla}^{(1)}\right)\sum_\alpha \phi_\alpha^{(1)} + \frac{1}{2}\left(\partial t^{(1)} + \vec{c}_\alpha.\vec{\nabla}^{(1)}\right)^2 \sum_\alpha \phi_\alpha^{(0)} = 0 \tag{A.13}$$

The last term on the LHS can be eliminated multiplying Eq. (A.10) by $\left(\partial t^{(1)} + \vec{c}_\alpha.\vec{\nabla}^{(1)}\right)$. The resulting equation is:

$$\left(\partial t^{(2)} + \vec{\nabla}^{(2)}.\vec{u}\right)\Xi + \vec{\nabla}^{(1)}\left(1 - \frac{1}{2\tau}\right)\sum_\alpha \vec{c}_\alpha \phi_\alpha^{(1)} = 0 \tag{A.14}$$

The last term appearing on the LHS is the first order moment of $\phi_\alpha^{(1)}$, which is not known. It can be evaluated by taking the first-order moment of Eq. (A.10):

$$\sum_\alpha \vec{c}_\alpha \phi_\alpha^{(1)} = -\tau \partial t^{(1)}\left(\sum_\alpha \vec{c}_\alpha \phi_\alpha^{(0)}\right) - \tau \vec{\nabla}^{(1)}.\left(\sum_\alpha \vec{c}_\alpha \otimes \vec{c}_\alpha \phi_\alpha^{(0)}\right) \tag{A.15}$$

Putting back Eq. (A.15) into Eq. (A.13):

$$\left(\partial t^{(2)} + \vec{\nabla}^{(2)}\vec{u}\right)\Xi + \vec{\nabla}^{(1)}.\left[\left(\frac{1}{2} - \tau\right)\partial t^{(1)}(\vec{u}\Xi) + c_s^2\left(\frac{1}{2} - \tau\right)\vec{\nabla}^{(1)}.\left(\Xi\bar{\bar{I}}\right)\right] = 0 \tag{A.16}$$

Now defining τ as:

$$\tau = \frac{\kappa}{c_s^2 \delta_t} + 0.5 \tag{A.17}$$

where κ is a generic physical parameter to be defined later, and adding up Eqs. (A.16) and (A.12) we get:

$$\left(\partial t + \vec{\nabla}.\vec{u}\right)\Xi - \vec{\nabla}.\left(\kappa\vec{\nabla}.\left(\Xi\bar{\bar{I}}\right)\right) - \frac{1}{c_s^2}\vec{\nabla}.\left(\kappa\partial t^{(1)}\vec{u}\Xi\right) = 0 \tag{A.18}$$

It is worth mentioning that keeping the two last terms in the fluid equilibrium distribution function would have resulted in additional spurious terms:

$$\vec{\nabla}^{(1)}\sum_\alpha \vec{c}_\alpha \otimes \vec{c}_\alpha \phi_\alpha^{(0)} = c_s^2\begin{bmatrix}\partial_x\Xi \\ \partial_y\Xi\end{bmatrix} + \begin{bmatrix}\partial_x\Xi u_x^2 + \partial_y\Xi u_x u_y \\ \partial_x\Xi u_x u_y + \partial_y\Xi u_y^2\end{bmatrix} \tag{A.19}$$

which would have eventually introduced the following error in the final equation:

$$E = \partial_x\left(\kappa\partial_x\Xi u_x^2 + \kappa\partial_y\Xi u_x u_y\right) + \partial_y\left(\kappa\partial_x\Xi u_x u_y + \kappa\partial_y\Xi u_y^2\right) \tag{A.20}$$

In the case of heat transport, the macroscopic scalar being transported is the temperature. Replacing the generic passive scalar Ξ with T, and the generic physical parameter κ by $\frac{\lambda}{\rho\bar{c}_p}$, the following equation is recovered at the macroscopic level:

$$\left(\partial t + \vec{\nabla}.\vec{u}\right)T - \vec{\nabla}.\left(\frac{\lambda}{\rho\bar{c}_p}\vec{\nabla}.\left(T\bar{\bar{I}}\right)\right) - \frac{1}{c_s^2}\vec{\nabla}.\left(\frac{\lambda}{\rho\bar{c}_p}\partial t^{(1)}\vec{u}T\right) = 0 \tag{A.21}$$

the second term on the LHS does not quite correspond to the macroscopic heat transfer equation as $\frac{1}{\rho\bar{c}_p}$ is now inside the gradient operator. Therefore, in addition to the last term on the LHS of Eq. (A.21), there is an error of the form:

$$E = -\left(\lambda\vec{\nabla}T\right).\left(\vec{\nabla}\frac{1}{\rho\bar{c}_p}\right) \tag{A.22}$$

For the species transport equation, assuming that we transport the mass fraction of species k, the passive scalar approach results in:

$$\left(\partial t + \vec{\nabla}.\vec{u}\right)Y_k - \vec{\nabla}.\left(D_k\vec{\nabla}Y_k\right) = 0 \tag{A.23}$$

which is equivalent to the species transport equation resulting from Fick's approximation. Two points however should be taken into account: (1) A velocity correction is needed, since both approximations from Fick or Hirschfelder and Curtiss lead to non-zero total diffusion velocity, (2) the density does not appear in the equation recovered by LB. The velocity correction term for the Fick approximation is:

$$\vec{V}^c = \sum_k D_k \vec{\nabla} Y_k \tag{A.24}$$

Assuming the last term on the LHS of Eq. (A.18) can be neglected, two correction terms must be added in order to recover the exact species conservation equations:

$$\left(\partial t + \vec{\nabla}.\vec{u}\right) Y_k - \vec{\nabla}.\left(D_k \vec{\nabla} Y_k\right) + \underbrace{\vec{\nabla}.\left(Y_k \sum_{k'} D_{k'} \vec{\nabla} Y_{k'}\right) - D_k \vec{\nabla} Y_k.\left(\frac{\vec{\nabla}\rho}{\rho}\right)}_{\text{correction}} = 0 \tag{A.25}$$

In the limit of weakly compressible flows with similar Lewis number Le for all species, these two last terms vanish. The extension of this demonstration to cases with a production term is straightforward.

Appendix B. REGATH-1D burner-stabilized formulation

The 1-D numerical approach of the REGATH package using a finite-difference solver is employed to study the structure of burner-stabilized ozone/air reacting flow. The governing equations describing the 1-D multi-species reactive flow are:

$$\rho u = \dot{m}, \tag{B.1}$$

$$\dot{m}\frac{\partial Y_k}{\partial x} = -\frac{\partial(\rho Y_k V_k)}{\partial x} + W_k\dot{\omega}_k, \tag{B.2}$$

$$\dot{m}c_p\frac{\partial T}{\partial x} = \frac{\partial}{\partial x}\Big(\lambda\frac{\partial T}{\partial x}\Big) - \sum_{k=1}^{N_{sp}}\rho Y_k V_k c_{p_k}\frac{\partial T}{\partial x} + \sum_{k=1}^{N_{sp}} W_k\dot{\omega}_k h_k, \tag{B.3}$$

where ρ is the density, u the velocity component in x direction, and $\dot{m}$ is a constant flow rate, $\dot{m} = \rho_0 u_0$, where the subscript 0 refers to fresh gas. Y_k represents the k^{th} species mass fraction. The diffusion velocity of the k^{th} species, V_k, is computed assuming complex transport phenomena. W_k is the k^{th} species molar mass and $\dot{\omega}_k$ represents the chemistry source term of the k^{th} species due to detailed combustion chemistry. T is the temperature, λ the mixture conductivity, c_p the mixture specific heat capacity, c_{p_k} the k^{th}species specific heat capacity, and h_k the k^{th} species enthalpy.

The presence of a burner is simulated by imposing the following boundary conditions at $x = 0$ for k^{th} species mass fraction and temperature :

$$Y_{k_{(x=0)}} + \frac{1}{\dot{m}}\Big(\rho Y_k V_k\Big)_{(x=0)} = Y_{k_0}, \tag{B.4}$$

$$T_{(x=0)} = T_0. \tag{B.5}$$

The boundary conditions at $x = L_f$ for k^{th} species mass fraction and temperature are:

$$\frac{\partial^2 Y_k}{\partial x^2} = 0, \tag{B.6}$$

$$\frac{\partial^2 T}{\partial x^2} = 0. \tag{B.7}$$

Appendix C. REGATH-1D counter-flow formulation

The 1-D formulation used in the standalone REGATH-1D solver for the counter-flow configuration assumes constant pressure by neglecting spatial pressure gradient. A cylindrical coordinate (y, r) is considered here. In addition, self-similarity assumption is used where only one-dimensional solution in the vicinity of the jet axis is formulated by assuming $u = U(y).r$, $\rho v = V(y)$ and $Y_k = Y_k(y)$. In these conditions, the pressure term becomes[49, 50]:

$$J = -\frac{1}{r}\frac{\partial p}{\partial r} = \text{constant} \tag{C.1}$$

and:

$$\frac{\partial J}{\partial y} = 0. \tag{C.2}$$

This model is based on the following system of equations:

$$\frac{\partial \rho}{\partial t} + (1+j)\rho U + \frac{(\partial \rho v)}{\partial y} = 0 \tag{C.3}$$

$$\frac{\partial (\rho U)}{\partial t} + \rho U^2 + \rho v \frac{\partial U}{\partial y} - J - \frac{\partial}{\partial y}\left(\mu \frac{\partial U}{\partial y}\right) = 0 \tag{C.4}$$

$$\rho \frac{\partial Y_k}{\partial t} + \rho v \frac{\partial Y_k}{\partial y} + \frac{\partial}{\partial y}\left(\rho Y_k V_k\right) - \dot{\omega}_k W_k = 0. \tag{C.5}$$

The corresponding boundary conditions at y=0 and y=L are:

$$U = 0 \tag{C.6}$$

$$\rho v = \rho_0 v_0 \tag{C.7}$$

$$Y_k = Y_{k,0} \tag{C.8}$$

$$T = T_0 \tag{C.9}$$

Where ρ_0, v_0, $Y_{k,0}$ and T_0 represent the values to be imposed at each boundary. Further details on the derivation and validation of this model can be found in [50, 51, 52, 53].

The solver used in REGATH-1D is a steady-state finite-difference solver. The system of equation is solved using the Newton-Raphson method.

Appendix D. Detailed kinetic scheme for an ozone/air reacting flow (from [44])

	$k = AT^{\beta}e^{-\frac{E}{RT}}$ for reaction:	A	β	E
1	$2O + M \leftrightarrow O_2 + M$	1.200000E+17	-1.000000E+00	0.000000E+00
2	$O_3 + O_2 \rightarrow O_2 + O + O_2$	1.540000E+14	0.000000E+00	2.305850E+04
3	$O_3 + O \rightarrow O_2 + O + O$	2.480000E+15	0.000000E+00	2.272160E+04
4	$O_3 + O_3 \rightarrow O_2 + O + O_3$	4.400000E+14	0.000000E+00	2.305850E+04
5	$O_3 + N_2 \rightarrow O_2 + O + N_2$	4.000000E+14	0.000000E+00	2.266190E+04
6	$O_2 + O + O_2 \rightarrow O_3 + O_2$	3.260000E+19	-2.100000E+00	0.000000E+00
7	$O_2 + O + N_2 \rightarrow O_3 + N_2$	1.600000E+14	-4.000000E-01	-1.390700E+03
8	$O_2 + O + O \rightarrow O_3 + O$	2.280000E+15	-5.000000E-01	-1.390700E+03
9	$O_2 + O + O_3 \rightarrow O_3 + O_3$	1.670000E+15	-5.000000E-01	-1.390700E+03
10	$O_2 + O_2 \rightarrow O + O + O_2$	9.800000E+24	-2.500000E+00	1.180382E+05
11	$O_2 + O \rightarrow O + O + O$	3.500000E+25	-2.500000E+00	1.180382E+05
12	$O_2 + O_3 \rightarrow O + O + O_3$	1.200000E+19	-1.000000E+00	1.180382E+05
13	$O + O + O_2 \rightarrow O_2 + O_2$	1.500000E+16	-4.000000E-01	0.000000E+00
14	$O + O + N_2 \rightarrow O_2 + N_2$	6.000000E+13	0.000000E+00	-1.789700E+03
15	$O + O + O \rightarrow O_2 + O$	5.340000E+16	-4.000000E-01	0.000000E+00
16	$O + O + O_3 \rightarrow O_2 + O_3$	1.300000E+14	0.000000E+00	-1.789700E+03
17	$O_2 + O_2 \rightarrow O_3 + O$	1.200000E+13	0.000000E+00	1.003871E+05
18	$O_3 + O \rightarrow O_2 + O_2$	4.820000E+12	0.000000E+00	4.095600E+03

The units of A, β and T are all based on moles, calories and seconds. M is used to represent an arbitrary third-body for the reaction.